Electronic Supplementary Material (ESI) for RSC Advances.
This journal is © The Royal Society of Chemistry 2016

Supplementary Information

Three-Dimensional Porous Carbon Nanosheet Networks Anchored with Cu_6Sn_5@Carbon as a High-Performance Anode Material for Lithium Ion Batteries

Zhiyuan Wang,*[a,b] Shaohua Luo, [a,b] Fang Chen,[a] Dan Wang, [a,b] Yanguo Liu, [a,b] Xiwei Qi, [a,b] Chunsheng Shi,[c] and Naiqin Zhao,[c]

[a] School of Resources and Materials, Northeastern University at Qinhuangdao, Qinhuangdao, China;

[b] Key Laboratory of Dielectric and Electrolyte Functional Material Hebei Province, Qinhuangdao, China;

[c] School of Materials Science and Engineering, Tianjin University, Tianjin 300072, P.R. China.

E-mail: zhiyuanwang@neuq.edu.cn;

Supplementary Figures

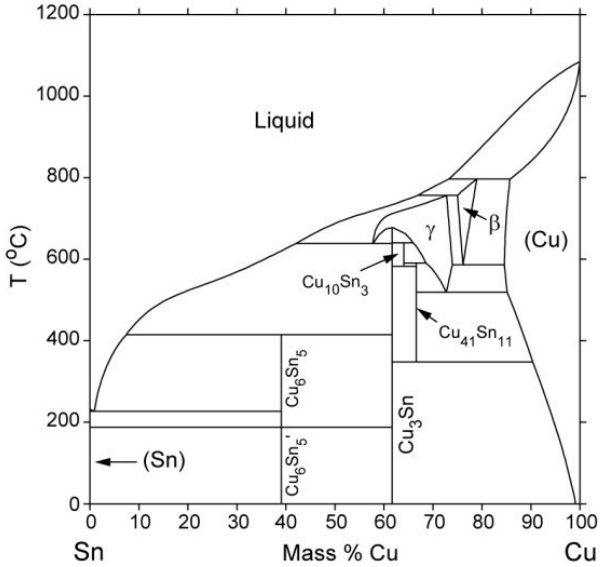

Fig. S1. The Cu-Sn phase diagram[1, 2].

To determine the contents of Cu_6Sn_5 and carbon in the composite, the 3D PCNNWs-Cu_6Sn_5@C composite was performed with thermogravimetric and differential thermal analysis (TG-DTA) in air, as shown in Figure S2. It is obvious that there was no notable weight loss from 25 to 265 °C, indicating that there is no oxidation reactions (Sn or Cu) and carbon decomposition bellow 265 °C and the composite is stable up to 265 °C in air. The weight decrease from 265 to

300 °C may be attributed to the oxidation of amorphous carbon, and the followed large weight loss from 300 to 475 °C is mainly due to carbon decomposition ($C + O_2 \rightarrow CO_2$) and accompanied by the oxidation of metallic copper and tin ($2Cu + O_2 \rightarrow 2CuO$; $Sn + O_2 \rightarrow SnO_2$). Thus, there is not mass increase ascribed to the oxidation of copper and tin can be observed because it is covered by the large mass decrease of carbon oxidation ($C + O_2 \rightarrow CO_2$). Because the Cu_6Sn_5 nanoparticles are embedded in carbon nanosheets and coated with carbon shells (Fig.3), so the oxidation of metallic copper and tin cannot occur before the oxidation of carbon layers. Assuming that the TG heating finally produces SnO_2 and CuO, the mass fraction of nano-Cu_6Sn_5 particles in the composite is determined to be 46.4% according to the following equation:

$$Cu_6Sn_5(wt\%) = \frac{final\ weight\ of\ product \times \frac{6}{11} \times \frac{M_{Cu}}{M_{CuO}} + final\ weight\ of\ product \times \frac{5}{11} \times \frac{M_{Sn}}{M_{SnO_2}}}{initial\ weight\ of\ 3D\ PCNNWs\text{-}Cu_6Sn_5@C\ composite} \times 100\% \quad \text{(S1-1)}$$

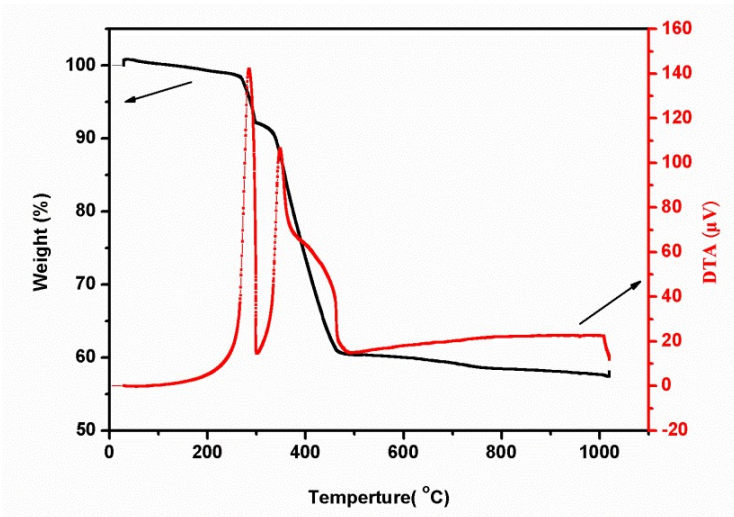

Fig. S2. TG-DTA curves of the 3D PCNNWs-Cu_6Sn_5@C composite in air.

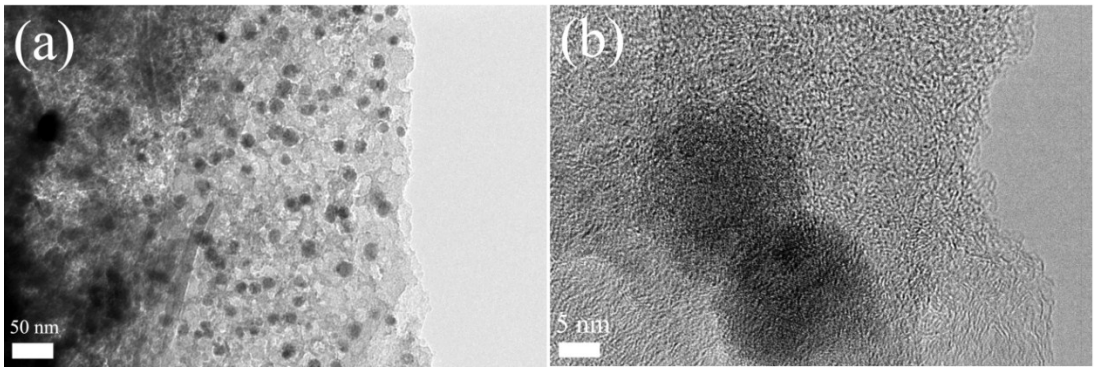

Fig. S3 Typical TEM images of 3D PCNNWs-Cu_6Sn_5@C electrode after 100 cycles with different magnification.

In order to identify if the unique architecture is stable after the repeated cycling, the cells after 100 cycles were disassembled in glove box, then the electrodes were washed with dimethyl carbonate (DMC) and dried in a vacuum drying oven at 80 ^{o}C for 10h. Finally, the anode material was scraped off and observed by TEM, as shown in Fig.3S. It is clearly that the Cu_6Sn_5 nanoparticles do not aggregate after repeated cycling and they are still homogeneously and firmly anchored on the surface of carbon nanosheets, which is almost the same as the morphology of the pristine product (Fig. 3b) except for the covered thick and gel-like SEI layer. This result indicates that the strong interaction between Cu_6Sn_5 nanoparticles and 3D carbon nanosheet networks as well as the superior mechanical flexibility of 3D porous carbon nanosheet networks, which can restrain the aggregation of Cu_6Sn_5 nanoparticles and the cracking of the electrode during charge/discharge cycling. As a result, the 3D PCNNWs-Cu_6Sn_5@C electrode displays an excellent cycling stability.

Supplementary Table

Table S1 Initial capacity, rate capability, and cycle performance for 3D PCNNWs-Cu_6Sn_5@C and some representative Cu-Sn alloy anodes in literatures.

Materials	1st charge capacity Capacity/rate (mAh g^{-1}/A g^{-1})	Cyclic Properties Capacity/current density/cycles (mAh g^{-1} /A g^{-1}/cycles)	Rate capability Current density: Capacity (A g^{-1}: mAh g^{-1})	Reference
3D porous carbon/Cu_6Sn_5	523 /0.2	366.4/1.0/200	1: 395 2: 327 5: 282	This work
3D porous Sn-Cu alloy/CNT	546.6//0.1	370.1/0.1/100	0.2: 365.5 0.8:225 1.6:175.9	S3
Graphene/Cu_6Sn_5	895 /0.2	330.9/0.5/100	1: 305 2: 270 5: 246	S4
Cu_3Sn_7	693.7/0.1	457.8/0.1/20	0.5: 429	S5
Cu_6Sn_5/Sn/Graphite	700 /0.1	605.8/0.1/100	0.5:150	S5
Carbon-coated Cu_6Sn_5	475 /0.1	383/0.1/50	—	S6
Porous Cu−Sn films	500 /0.05	300/0.05/80	—	S7
RGO/Cu_6Sn_5 composite	456/0.1	402 /0.1/250	—	S8

Reference

(S1) S. Fürtauer, D. Li, D. Cupid, H. Flandorfer, The Cu–Sn phase diagram, Part I: New experimental results. Intermetallics, 2013, 34, 142-147.

(S2) D. Li, P. Franke, S. Fürtauer, D. Cupid, H. Flandorfer, The Cu–Sn phase diagram, Part II: New thermodynamic assessment. Intermetallics, 2013, 34, 148-158.

(S3) X. Y. Fan, Y. X. Shi, Y. Cui, D. L. Li, L. Gou, Ionics, 2015, 21, 1909-1917.

(S4) J. Z. Chen, L. Yang, S. H. Fang, Z. X. Zhang and S. I. Hirano, Electrochim. Acta, 2013, 105, 629-634.

(S5) Q. G. Han, Z. Yi, Y. Cheng, Y. M. Wu, L.M. Wang, RSC Adv., 2016, 6, 15279-15285.

(S6) W. J. Cui, F. Wang, J. Wang, H. J. Liu, C. X. Wang and Y. Y. Xia, J. Power Sources, 2011, 196, 3633-3639.

(S7) D. B. Polat, J. Lu, A. Abouimrane, O. Keles and K. Amine, ACS Appl. Mater. Inter., 2014, 6, 10877-10885.

(S8) F. Wang, J. Yi, Y. G. Wang and Y. Y. Xia, Nanotechnology, 2013, 24, 424010-424014.